



Supplement of

Modelling the effect of aerosol and greenhouse gas forcing on the South Asian and East Asian monsoons with an intermediate-complexity climate model

Lucy G. Recchia and Valerio Lucarini

Correspondence to: Lucy G. Recchia (l.g.recchia@reading.ac.uk)

The copyright of individual parts of the supplement might differ from the article licence.

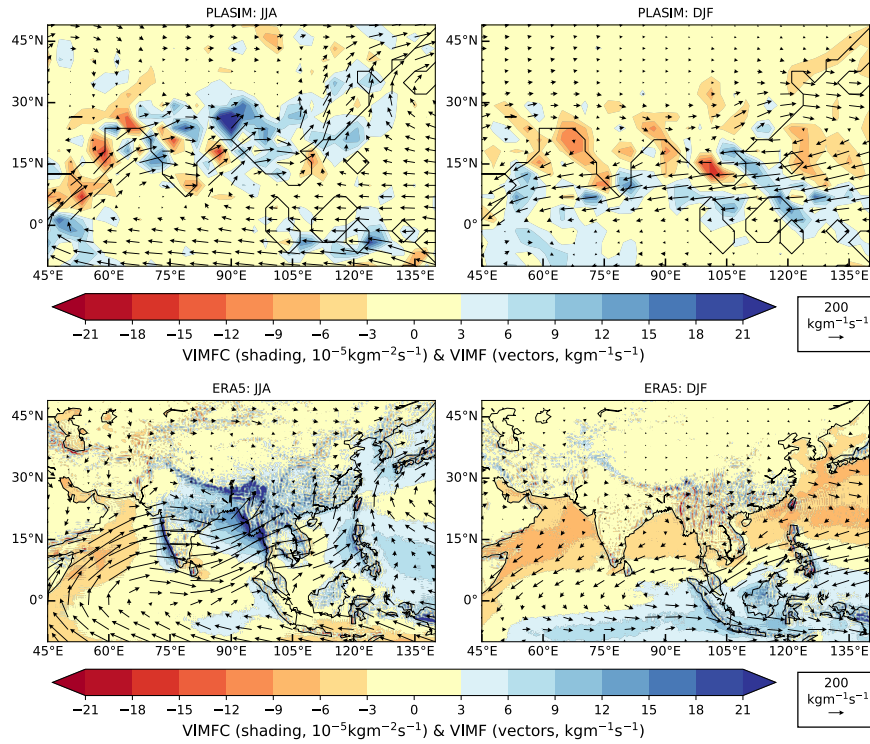


Figure S1. Vertically integrated moisture flux convergence (VIMFC, shading) and vertically integrated moisture flux (VIMF, vectors), averaged over June-July-August (left column) and December-January-February (right column). Top row shows data from 100-year PLASIM control run. Bottom row shows data from ERA5 reanalysis (Copernicus Climate Change Service, 2017) for period 1988–2017.

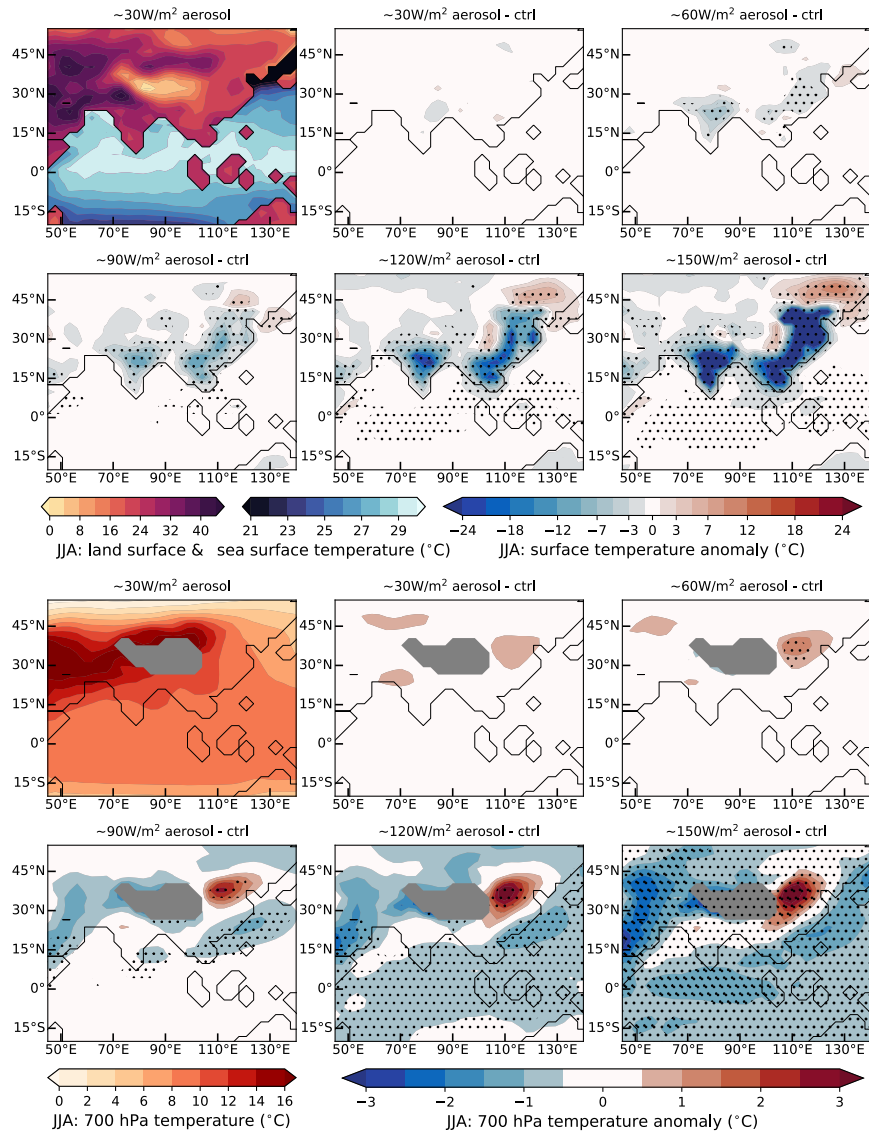


Figure S2. *Aerosol only* simulation. Contours showing mean decadal June-July-August temperature and mean decadal June-July-August temperature anomaly compared to the control run (anomaly = *aerosol only* - control), for a range of aerosol forcing values. The top two rows are at the surface and the bottom two rows at 700 hPa. Areas of high orography are masked in grey. Stippling where the anomaly exceeds double the JJA interannual variability.

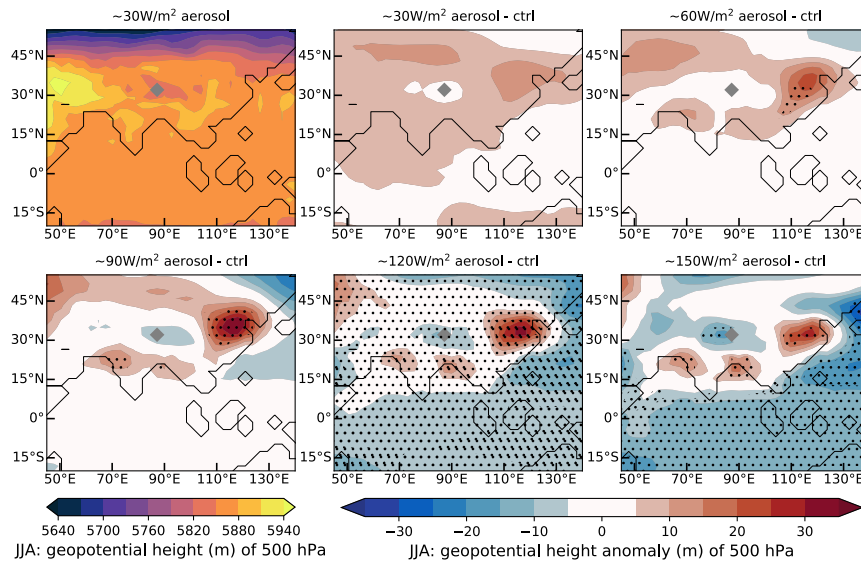


Figure S3. *Aerosol only* simulation. Contours showing mean decadal June-July-August 500 hPa geopotential height and mean decadal June-July-August 500 hPa geopotential height anomaly compared to the control run (anomaly = *aerosol only* - control), for a range of aerosol forcing values. Areas of high orography are masked in grey. Stippling where the anomaly exceeds double the JJA interannual variability.

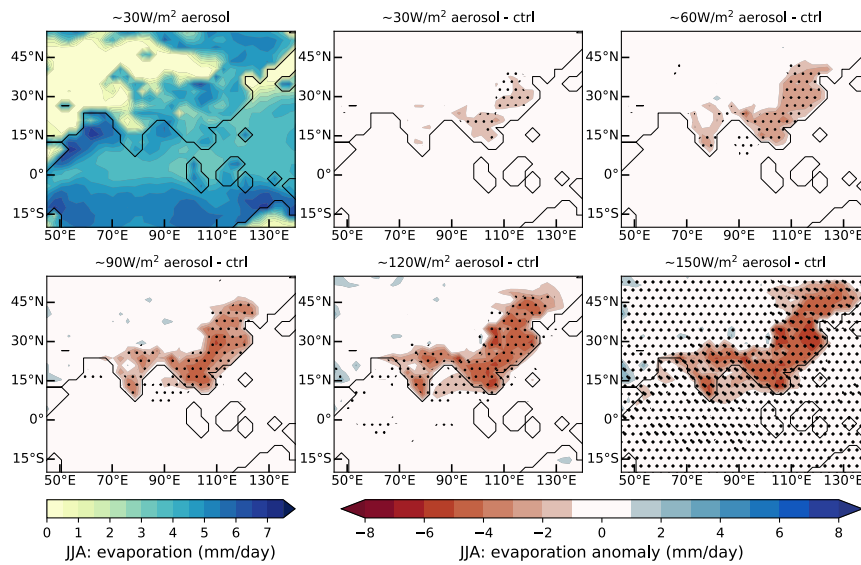


Figure S4. *Aerosol only* simulation. Contours showing mean decadal June-July-August evaporation and mean decadal June-July-August evaporation anomaly compared to the control run (anomaly = *aerosol only* - control), for a range of aerosol forcing values. Stippling where the anomaly exceeds double the JJA interannual variability.

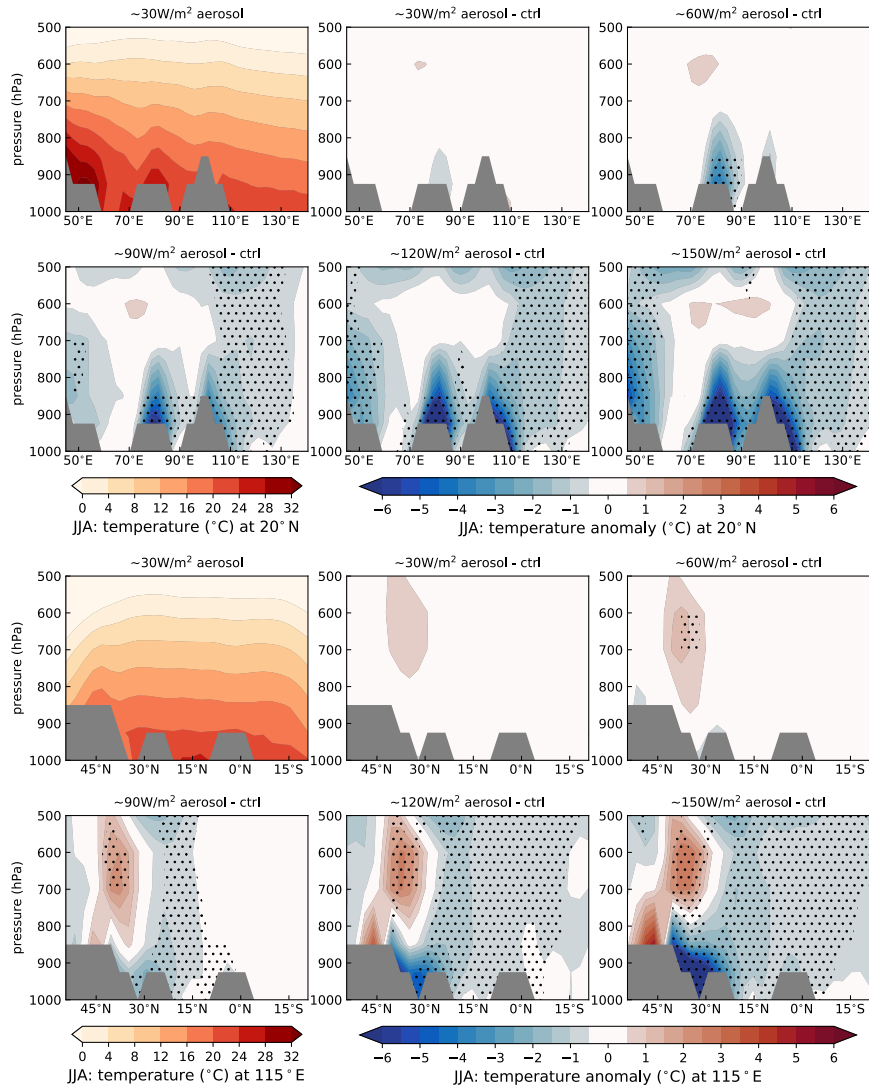


Figure S5. *Aerosol only* simulation. Vertical section along 20°N (top two rows) and 115°E (bottom two rows) with contours showing mean decadal June-July-August temperature & temperature anomaly, compared to control run (anomaly = *aerosol only* - control), for a range of aerosol forcing values. Areas of high orography are masked in grey. Stippling where the anomaly exceeds double the JJA interannual variability.

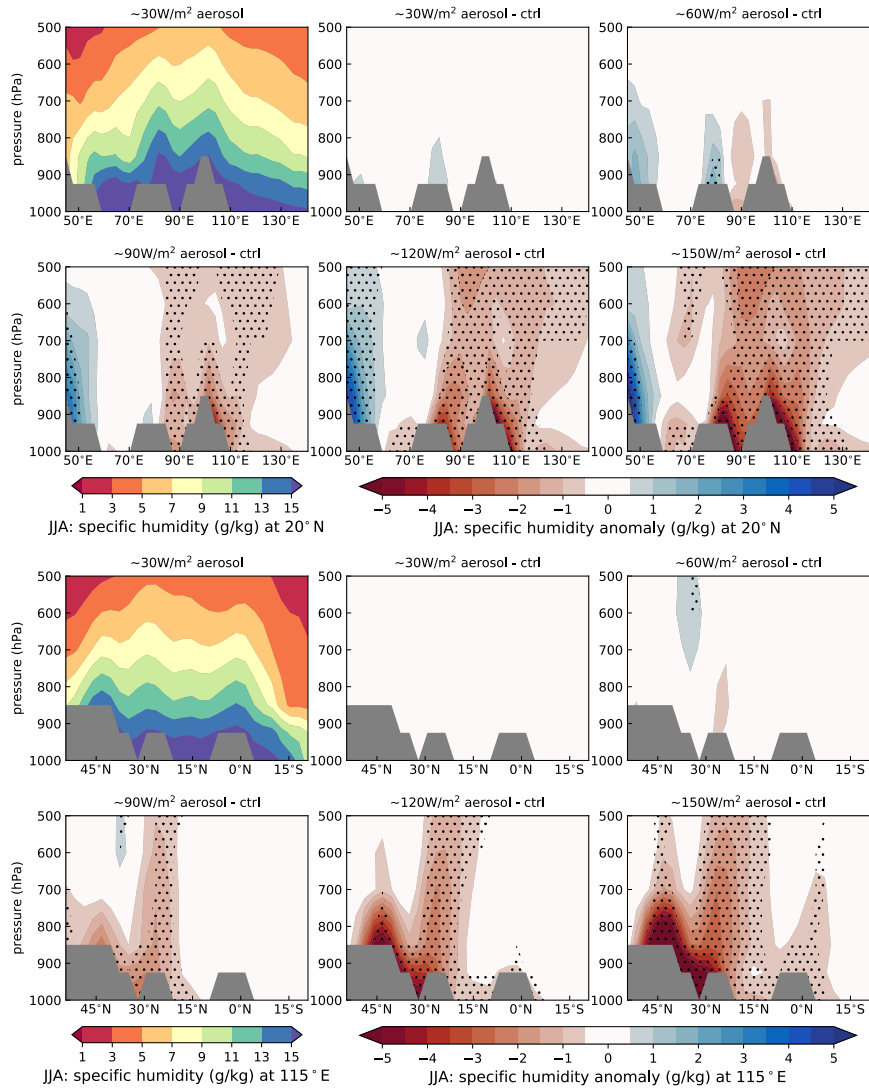


Figure S6. *Aerosol only* simulation. Vertical section along 20°N (top two rows) and 115°E (bottom two rows) with contours showing mean decadal June-July-August specific humidity & specific humidity anomaly, compared to control run (anomaly = *aerosol only* - control), for a range of aerosol forcing values. Areas of high orography are masked in grey. Stippling where the anomaly exceeds double the JJA interannual variability.

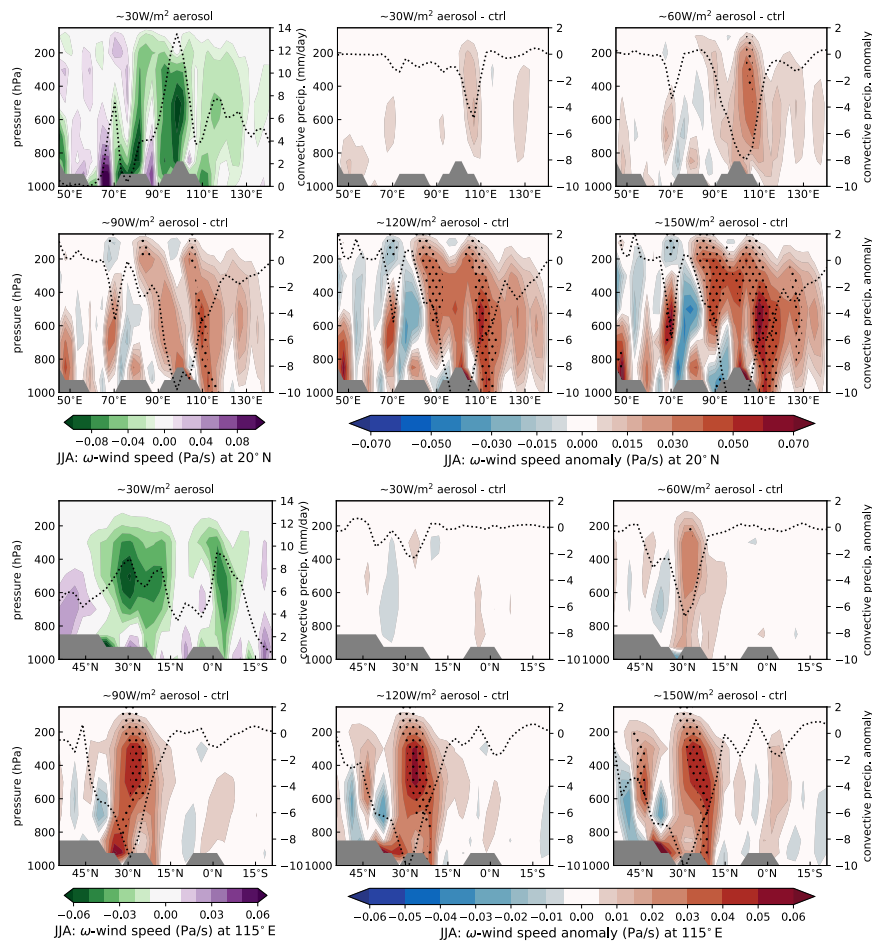


Figure S7. *Aerosol only* simulation. Vertical section along 20°N (top two rows) and 115°E (bottom two rows) with contours showing mean decadal June-July-August vertical velocity (ω) & vertical velocity anomaly, compared to control run (anomaly = *aerosol only* - control), for a range of aerosol forcing values. Dotted lines show the convective precipitation/convective precipitation anomaly along the section. Areas of high orography are masked in grey. Stippling where the anomaly exceeds double the JJA interannual variability.

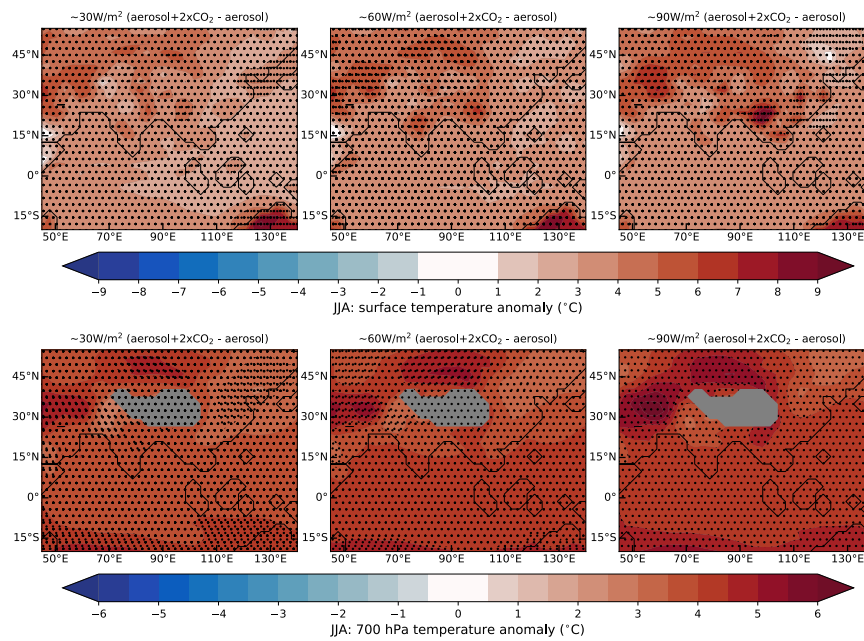


Figure S8. *Aerosol with 2xCO₂* simulation. Contours showing mean decadal June-July-August surface (top row) & 700 hPa (bottom row) temperature anomaly, compared to *aerosol only* run (anomaly = *aerosol with 2xCO₂* - *aerosol only*), for a range of aerosol forcing values. Areas of high orography are masked in grey. Stippling where the anomaly exceeds double the JJA interannual variability.

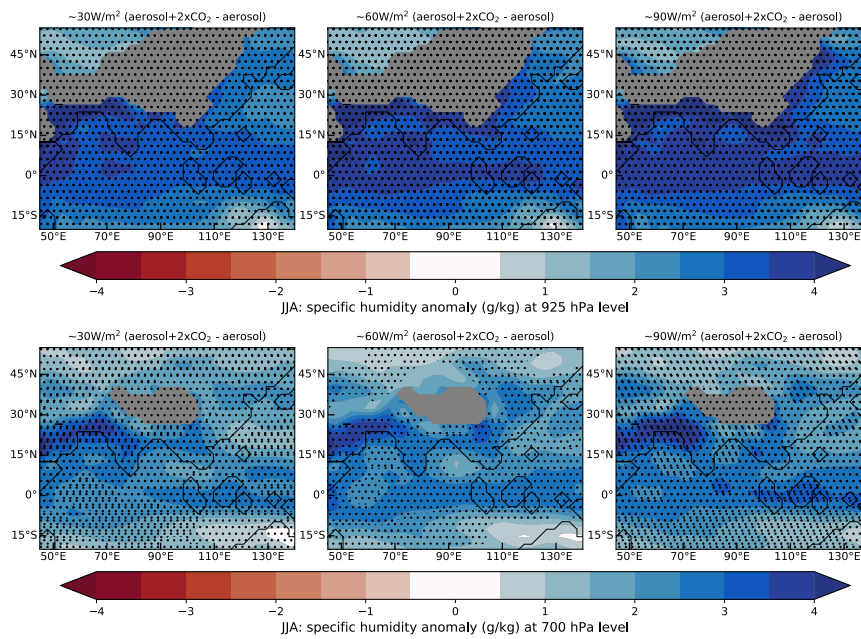


Figure S9. *Aerosol with 2xCO₂*. Contours showing mean decadal June-July-August 925 hPa (top row) & 700 hPa (bottom row) specific humidity anomaly, compared to *aerosol only* run (anomaly = *aerosol with 2xCO₂* - *aerosol only*), for a range of aerosol forcing values. Areas of high orography are masked in grey. Stippling where the anomaly exceeds double the JJA interannual variability.

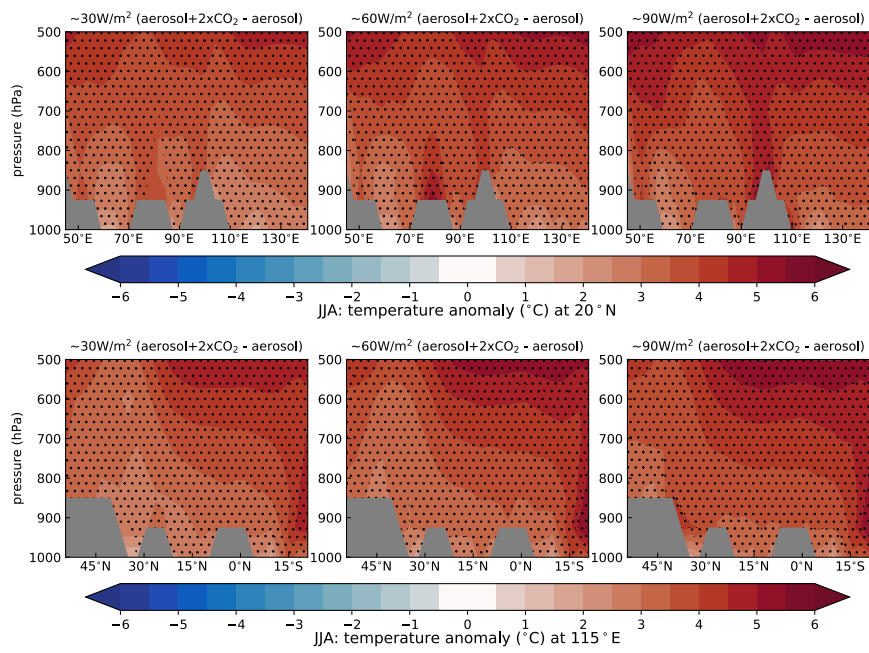


Figure S10. *Aerosol with 2xCO₂* simulation. Vertical section along 20°N (top two rows) and 115°E (bottom two rows) with contours showing mean decadal June-July-August temperature anomaly, compared to *aerosol only* run (anomaly = *aerosol with 2xCO₂* - *aerosol only*), for a range of aerosol forcing values. Areas of high orography are masked in grey. Stippling where the anomaly exceeds double the JJA interannual variability.

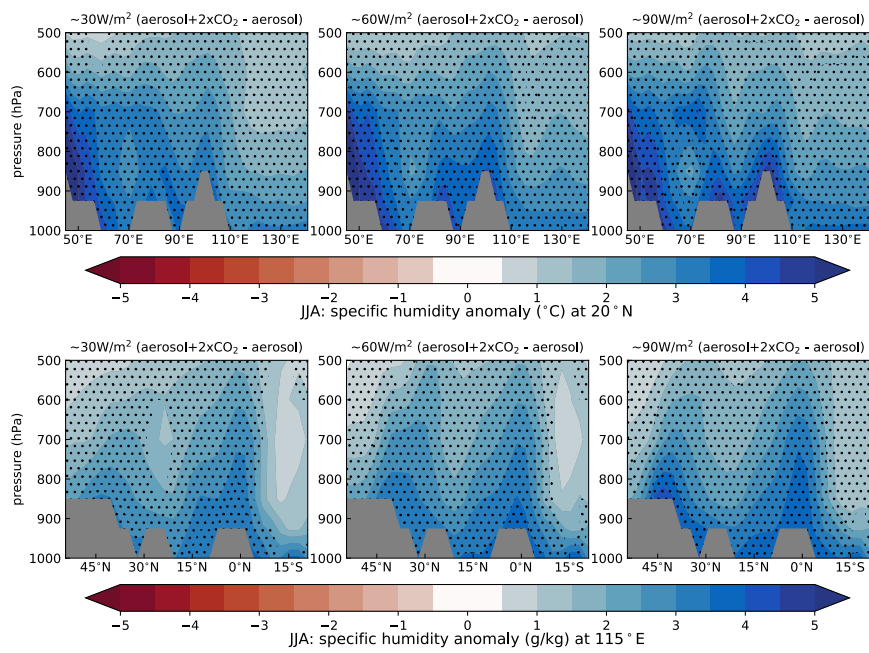


Figure S11. *Aerosol with 2xCO₂* simulation. Vertical section along 20°N (top two rows) and 115°E (bottom two rows) with contours showing mean decadal June-July-August specific humidity anomaly, compared to *aerosol only* run (anomaly = *aerosol with 2xCO₂* - *aerosol only*), for a range of aerosol forcing values. Areas of high orography are masked in grey. Stippling where the anomaly exceeds double the JJA interannual variability.

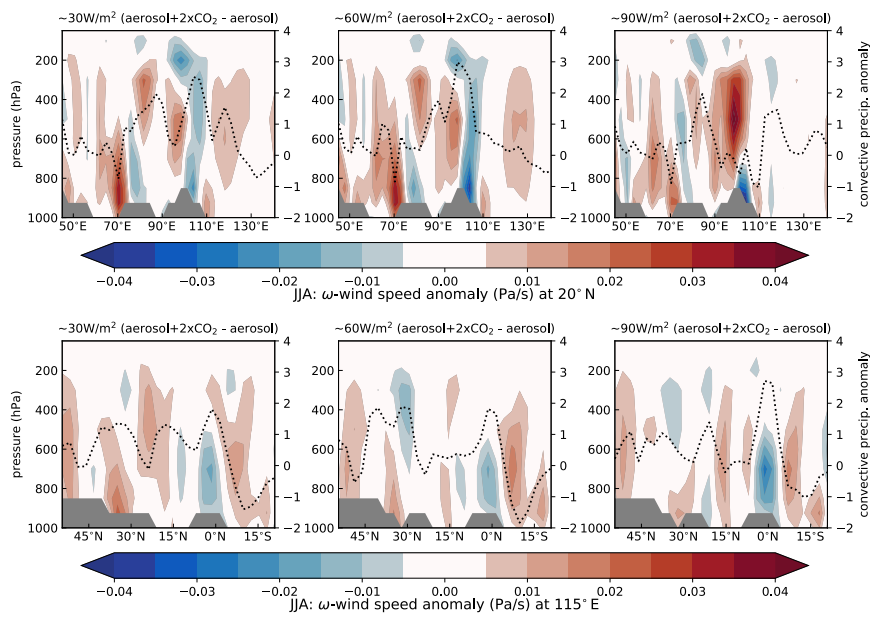


Figure S12. *Aerosol with 2xCO₂* simulation. Vertical section along 20°N (top row) and 115°E (bottom row) with contours showing mean decadal June-July-August vertical velocity (ω) & vertical velocity anomaly, compared to *aerosol only* run (anomaly = *aerosol with 2xCO₂* - *aerosol only*), for a range of aerosol forcing values. Dotted lines show the convective precipitation/convective precipitation anomaly along the section. Areas of high orography are masked in grey. Stippling where the anomaly exceeds double the JJA interannual variability.